

# Influence of Dust Layers in Connecting Pipes on Explosion Propagation Characteristics of Flake Aluminum Powder in Cylindrical Interconnected Vessels

Dan Wang,<sup>§</sup> Qi Jing,<sup>§</sup> and Yulong Cheng\*Cite This: *ACS Omega* 2023, 8, 2197–2212

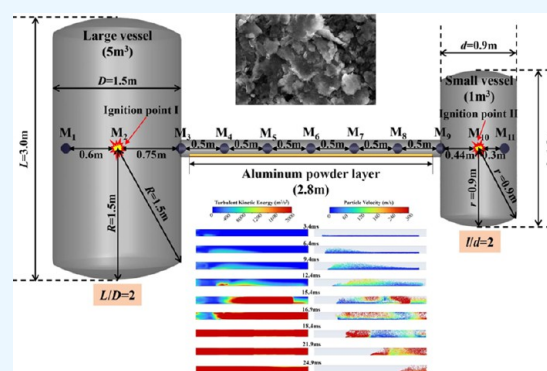
Read Online

ACCESS |

Metrics &amp; More

Article Recommendations

**ABSTRACT:** Aluminum dust explosion has become an important type of dust explosion accident. In the present work, an interconnected system is established to study the influence of accumulated dust layers in connecting pipes on explosion propagation characteristics. A high-precision computational fluid dynamics (CFD) method is applied to study the overpressure and flame development of aluminum powder explosion under the central ignition condition of two cylindrical vessels with a volume ratio of 1:5. The results show that pressure build-up in the secondary container is mainly due to the oscillating pressure wave. Moreover, compared with the ignition container, the thickness of the dust layer has a more obvious enhancement effect on the peak overpressure for the secondary container. When the ignition occurs in a large container, the dust layer is lifted in the connecting pipe under the action of the precursor pressure wave. After the jet flame enters the connecting pipe, the lifted aluminum dust participates in the explosion reaction, which significantly increases the explosion intensity. With the participation of the accumulated dust layer, the maximum overpressure of the explosion of flake aluminum dust in the interconnected system is higher than 30 bar, and the jet flame velocity is increased by 3 times. The present work can provide reference for the safety design of process equipment involving dust.



## 1. INTRODUCTION

In recent years, aluminum powder explosion accident has become the main type of dust explosion accident, causing serious consequences. For example, the “11·20” explosion accident in Guangdong, China, in 2012 was caused by an electrostatic spark igniting the deposited aluminum powder layer in a ventilation duct. In 2014, the “8.2” explosion accident in Jiangsu, China, was caused by the explosion of aluminum powder due to complex environmental conditions of high temperature and high humidity. In addition, in the dust processing industry, the containers for storing various explosive dusts are often connected to each other through pipes to form an interconnecting system.<sup>1</sup> Sparks caused by static electricity or friction can ignite dust cloud in a vessel (referred to as an ignition vessel), and flame and pressure wave propagates through a connecting pipe. As the flame enters the pipe from the ignition vessel, the change in geometry results in an acceleration of the flame front.<sup>2,3</sup> In addition, when there is an accumulated dust layer in the connecting pipe, the shock wave could lift the deposited dust layer into the adjacent vessel (referred to as a secondary vessel). Under the combined action of the jet flame and the pressure accumulation effect, more violent secondary explosion occurs in the secondary vessel, resulting in more serious consequences than the primary

explosion.<sup>4</sup> Therefore, it is of great significance to the structural design of interconnected vessels to study the enhancement law of the dust layer on the flame propagation and pressure change of the dust explosion.<sup>5</sup>

Researchers have carried out many studies on the process of gas or dust explosion in closed vessels and tubes, and many research results have also been published.<sup>5–7</sup> In addition, some researchers have carried out many experiments and simulation on the explosion overpressure characteristics of connected systems, and they have analyzed the explosion characteristics of gas or dust in closed systems. The effects of the vessel size, initial concentration, ignition position, and pressure relief conditions on explosion were preliminarily studied, and the similarities and differences between the independent vessel and the connected system were compared.<sup>8–11</sup> Jiang and co-workers<sup>12</sup> found that the explosion in interconnected vessels has a strong destructive power to the secondary vessel, especially the explosion

Received: October 4, 2022

Accepted: December 22, 2022

Published: January 4, 2023



propagation from a large vessel to a small vessel. When ignition occurs in a large vessel, the peak overpressure of the secondary vessel increases with the length of the connecting pipe. The peak overpressure for both vessels shows an approximately linear function of the initial pressure. Kosinski et al.<sup>3,13</sup> used the Euler–Lagrange method to simulate the consequences of a dust explosion in two vessels connected by a pipe. It was found that the probability of the explosion propagating from the ignition vessel to the secondary vessel decreased with decrease in the pipe diameter and increase in the pipe length. Reding and Shiflett<sup>14</sup> found that organic dust deflagration exhibits jet flame and pressure build-up phenomena when dust explosions propagated between interconnected containers, resulting in pressure wave oscillations and elevated explosion pressure peaks. Boeck et al.<sup>15</sup> developed a numerical model based on explosion dynamics that takes into account combustion within interconnected vessels, flame jets, external explosions caused by ventilation, and accelerated flame propagation within the connecting pipe. Huang and co-workers<sup>16</sup> studied the effect of venting membranes on the explosion characteristics of methane–air mixtures in interconnected vessels. They found that the thinner the venting membrane or the smaller the blockage rate, the lower the explosion overpressure. In addition, they observe a secondary explosion in the ventilation duct, but as the blockage rate increases, the flame becomes extremely weak, and the secondary explosion phenomenon gradually disappears. Song and Zhang<sup>17</sup> studied the propagation characteristics of secondary explosions of dust cloud in a closed tube. Our previous studies<sup>18–21</sup> have shown the overpressure characteristics and two-phase flow law of gas explosions and gas-powder hybrid system explosions in a closed vessel and proposed a complete numerical calculation method for two-phase explosions.

Moreover, some exploratory work has been done on the study of dust explosion in interconnected vessels. It was shown that the point in time at which an explosion can occur in the secondary vessel is a function of the duct height and particle size.<sup>22</sup> Reding and Shiflett<sup>14</sup> considered an accelerated flame front may result in flame jet ignition within the secondary vessel, and they found according to relative enclosure volumes, relief area, fuel type, suspended concentration, duct size, and duct length, the maximum system pressure in both interconnected vessels can be unpredictable. Moreover, the effect of the pipe bending angle on pressure piling in coal dust explosion in fully enclosed interconnected vessels was studied, including the effect on the instantaneous pressure spike, the rate of pressure rise, and the residual pressure in the interconnected system.<sup>1</sup> In addition, the explosion characteristics of the deposited dust layer are also worthy of attention. Song et al.<sup>23,24</sup> simulated the process of premixed methane explosion igniting deposited coal/inert rock dust at the bottom of a tube and the flame propagation of dust layer explosion induced by weak ignition. They found that the deposited dust amount, particle size, and dust layer thickness have an influence on the dust explosion parameters. Pang et al.<sup>25,26</sup> designed a cylindrical and square vessel connected with a vent duct and analyzed the dynamic mechanism of dust explosion through a vent duct. Dong et al.<sup>27</sup> investigated methane–air explosions in a horizontal pipe closed at both ends with the deposited coal dust. It was found that the amplitude of pressure fluctuation was reduced when deposited coal dust was paved in the bottom of the pipe.<sup>28</sup>

The dust explosion in a closed container has a short duration and a fast rise rate of pressure, so there is a certain danger in

experiments. In addition, due to the limitation of experimental space and cost, the current explosion experimental research on the connected system cannot provide a large amount of general data to guide the design of the container. Therefore, in this paper, the computational fluid dynamics (CFD) method is used to study the overpressure and the flame development process of aluminum dust explosion in interconnected containers under the central ignition condition of two cylindrical containers with different volumes. The influence of the dust layer deposited in the connecting pipe on the jet flame and pressure accumulation is explored. The results can provide reference for the safety design, explosion venting, and explosion-proof parameters of dust-type chemical plants.

## 2. METHOD DETAILS

### 2.1. Numerical Algorithms and Governing Equations.

The flake aluminum dust explosion involves a complicated gas-dust two-phase flow, so we expound the gas-dust heterogeneous flow and flake aluminum dust combustion based on the following assumptions: (1) Flake aluminum particles were regarded as equal-sized cylinders with a base area of 14.21  $\mu\text{m}^2$  and a height of 1.8  $\mu\text{m}$ . (2) A simplified one-step reaction was used for aluminum dust combustion,  $\text{Al} + 3/4\text{O}_2 \rightarrow 1/2\text{Al}_2\text{O}_3 + 1675 \text{ kJ}$ . (3) Aluminum oxide ( $\text{Al}_2\text{O}_3$ ) was assumed as the gas phase. (4) Interactions between the discrete phase and the continuous gas phase in the diffusion process were considered, as well as the interphase exchange of heat, mass, and momentum. (5) Gaseous phase was assumed to be viscous and compressible.

The ANSYS-Fluent 2022R1 software was applied to solve the current numerical model. The combustion process of flake aluminum dust is a complicated multiphase flow process. The finite volume method (FVM) is used to solve the N–S equations involving the conservation of momentum, energy, and mass. Considering the micron-sized aluminum dust particles as discrete phases, the numerical algorithm needs to add the kinetic model, mass transfer model, heat transfer model, and chemical reaction model between the particle phase and gas phase. The pressure–velocity coupling algorithm adopts the third-order precision PISO algorithm, and the MUSCL interpolation algorithm is used for the flow term to improve the calculation accuracy.<sup>29</sup>

Mass conservation equation:

$$\frac{\partial \rho}{\partial t} + \frac{\partial(\rho u_i)}{\partial x_i} = S_k \quad (1)$$

Momentum conservation equation:

$$\frac{\partial(\rho u_i)}{\partial t} + \frac{\partial(\rho u_i u_j)}{\partial x_j} = -\frac{\partial p}{\partial x_i} + \frac{\partial \tau_{ij}}{\partial x_j} + \rho g_i + F_i \quad (2)$$

$$\tau_{ij} = -\frac{2}{3}\mu \frac{\partial u_k}{\partial x_k} \delta_{ij} + \mu \left( \frac{\partial u_i}{\partial x_j} + \frac{\partial u_j}{\partial x_i} \right) \quad (3)$$

Energy conservation equation:

$$\begin{aligned} \frac{\partial(\rho E)}{\partial t} + \frac{\partial[(\rho E + p)u_i]}{\partial x_i} \\ = \frac{\partial \left( K_{\text{eff}} \frac{\partial T}{\partial x_i} - \sum_j h_j \vec{J}_j' + u_j (\tau_{ij})_{\text{eff}} \right)}{\partial x_i} + S_h \end{aligned} \quad (4)$$

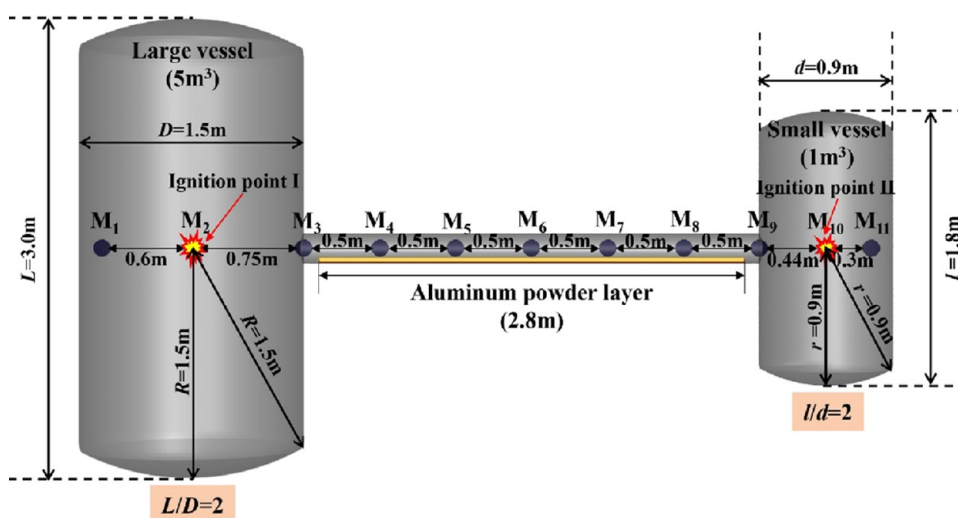


Figure 1. Interconnected containers model and monitoring points location.

$$E = h - \frac{p}{\rho} + \frac{u_i^2}{2} \quad (5)$$

The turbulence model adopts the standard  $k - \omega$  model, so the turbulence kinetic energy ( $k$ ) and the specific dissipation rate ( $\omega$ ) are obtained from the following transport equations ( $x$ -direction):<sup>30</sup>

$$\frac{\partial}{\partial t}(\rho k) + \frac{\partial}{\partial x_i}(\rho k u_i) = \frac{\partial}{\partial x_j} \left( \Gamma_k \frac{\partial k}{\partial x_j} \right) + G_k - Y_k \quad (6)$$

$$\frac{\partial}{\partial t}(\rho \omega) + \frac{\partial}{\partial x_i}(\rho \omega u_i) = \frac{\partial}{\partial x_j} \left( \Gamma_\omega \frac{\partial \omega}{\partial x_j} \right) + G_\omega - Y_\omega \quad (7)$$

where  $u$  is the gas velocity;  $G_k$  is the generation of turbulence kinetic energy due to mean velocity gradients;  $G_\omega$  is the generation of  $\omega$ ;  $\Gamma_k$  and  $\Gamma_\omega$  represent the effective diffusivity of  $k$  and  $\omega$ , respectively;  $Y_k$  and  $Y_\omega$  represent the dissipation of  $k$  and  $\omega$  due to turbulence, respectively.

The particle trajectory is solved by integrating the particle force differential equation in the pull-type coordinates, and the Stochastic Tracking model is applied.<sup>31</sup> The specific form ( $x$ -direction) of the particle force balance equation in the Cartesian coordinate system is as follows:

$$\frac{\partial}{\partial t}(u_p) = F_D(u - u_p) + \frac{g_x}{\rho_p}(\rho_p - \rho) + F_x \quad (8)$$

where  $u_p$  is particle velocity;  $F_D(u - u_p) = \frac{18\mu C_D Re}{24\rho_p d_p^2(u - u_p)}$  is the drag force on the particle per unit mass;  $Re$  is the relative Reynolds number;  $\rho_p$  is the particle density;  $d_p$  is the particle diameter; and  $F_x = \frac{1}{2} \frac{\rho}{\rho_p} \frac{d}{dt}(u - u_p)$  is the additional mass force of the particle.

$C_D$  is the dimensionless drag coefficient. A particle shape factor is defined to calculate the drag coefficient of nonspherical particles, and  $\sigma_s$  is 0.4056 for the present flake aluminum particles.<sup>32</sup>

$$C_D = \frac{24}{Re} (1 + \delta_1 Re^{\delta_2}) + \frac{\delta_3 Re}{\delta_4 + Re} \quad (9)$$

$$\delta_1 = \exp(2.3288 - 6.4581\sigma_s + 2.448\sigma_s^2)$$

$$\delta_2 = 0.0964 + 0.5565\sigma_s$$

$$\delta_3 = \exp(4.905 - 13.8944\sigma_s + 18.4222\sigma_s^2 - 10.2599\sigma_s^3)$$

$$\delta_4 = \exp(1.4681 - 12.2584\sigma_s - 20.7322\sigma_s^2 + 15.8855\sigma_s^3) \quad (10)$$

The kinetics/diffusion model was adopted for the surface combustion process of flake aluminum particles. The surface combustion rate is determined by a kinetics rate  $\mathfrak{R}$  and a diffusion rate  $D_0$ , which are as follows:

$$\frac{dm_p}{dt} = -\pi d_p^2 P_{Ox} \frac{D_0 \mathfrak{R}}{D_0 + \mathfrak{R}} \quad (11)$$

$$D_0 = C_1 \frac{[(T_p + T_\infty)/2]^{0.75}}{d_p} \quad (12)$$

$$\mathfrak{R} = A_s e^{(-E_s/RT_p)} \quad (13)$$

Here, the parameters of  $C_1$ ,  $A_s$ , and  $E_s$  are  $7.5 \times 10^{-10}$ , 0.02, and  $5.4 \times 10^6$  J/kmol, respectively.

The momentum value transferred from the continuous phase to the discrete phase is solved by calculating the momentum change of the particle as it passes through each computational grid.<sup>20</sup> The momentum exchange equation is as follows:

$$F = \sum \left[ \frac{118}{24\rho_p d_p^2} (u_p - u) \right] \dot{m}_p \Delta t \quad (14)$$

where  $\dot{m}_p$  is the particle mass flow and  $\Delta t$  is the time step.

The energy exchange equation between the granular phase and the continuous phase is

$$m_p c_p \frac{dT_p}{dt} = h A_p (T_\infty - T_p) + \varepsilon_p A_p \sigma (\theta_R^4 - T_p^4) \quad (15)$$

where  $T_p$  is the particle temperature;  $m_p$  is the particle mass;  $c_p$  is the particle heat capacity;  $A_p$  is the particle surface area;  $T_\infty$  is the gas-phase temperature;  $h$  is the convective heat transfer coefficient;  $\varepsilon_p$  is the particle emissivity;  $\sigma$  is the Stefan–

Boltzmann constant; and  $\theta_R$  is the temperature of the radiation source.

**2.2. Physical Model and Mesh Validation.** A geometric model shown in Figure 1 is established in this study. A large cylindrical container of 5 m<sup>3</sup> and a small cylindrical container of 1 m<sup>3</sup> are connected by a pipe with a diameter of 0.2 m and a length of 3 m, and both the length diameter ratio (L/D) of the two cylindrical containers is 2:1. In order to study the two flame propagation characteristics, two ignition modes are set up. Ignition mode I is that the large container is evenly filled with aluminum dust clouds and the small container is not filled with dust, and the ignition point is at the center of the large container. Ignition mode II is that the small container is evenly filled with aluminum dust clouds and the large container is not filled with dust, and the ignition point is at the center of the small container. It should be noted that the dust cloud concentration in the initiation container is directly set as the initial condition during initialization. The upper wall and lower wall of the connecting pipe are set with boundary conditions. The upper wall is always set as the "Wall" boundary, while the lower wall is first set as the "Pressure Inlet" boundary. The aluminum powder is sprayed into the connecting pipe at a very low velocity ( $1 \times 10^{-10}$  m/s). When the total amount of dust reaches the design value, the lower wall is changed to the "Wall" boundary, and the amount of dust does not increase. After standing for 10 min, the dust in the connecting pipe can be evenly laid on the lower wall of the pipe. The aluminum dust layer is laid at the bottom of the connecting pipe with a length of 2.8 m. Eleven monitoring points are set along the axis of the connecting pipe to monitor the characteristic parameters during the explosion process. Some important parameters in simulation are summarized in Table 1.

**Table 1. Constant Parameters of Simulation**

parameter	value
ignition energy	100 J
ignition radius	0.005 m
minimum cell size	1 mm
grid number	50034
particle scattering factor	0.9
particle emissivity	0.4
combustion heat of aluminum dust	$3.25 \times 10^7$ J/kg
aluminum dust density	2375 kg/m <sup>3</sup>

There is no uniform standard for the ignition energy on studying dust explosion, and the traditional method is more inclined to use chemical ignition heads. However, chemical ignition heads have many shortcomings. For example, the ignition process cannot be monitored in detail, the effective ignition energy cannot be accurately evaluated, and there are serious safety hazards in the use process. On the contrary, the ignition method of electric spark can more accurately control the discharge process of ignition energy, and we can accurately calculate the effective ignition energy.

The ignition system in the present study consists of a spark electrode and a capacitor discharge device. According to the Kirchoff law, the passive RLC discharge circuit satisfies the following relationship:

$$i(t) = \frac{U_0}{\omega L} e^{-t/\tau} \sin \omega t_d$$

$$\tau = \frac{2L}{R}$$

$$\omega = \left( \frac{1}{LC} - \frac{1}{\tau^2} \right)^{1/2} \quad (16)$$

The discharge power of the electric spark ( $P$ ) and the accumulated discharge energy ( $E$ ) can be obtained according to the following equations:

$$P = i^2(t)R_{\text{spark}} \quad (17)$$

$$E = \int i^2(t)R_{\text{spark}} dt \quad (18)$$

where  $R_{\text{spark}}$  is the equivalent resistance of the spark. The parameter curves of the discharge process with an ignition energy of 100 J are shown in Figure 2, from which it can be found

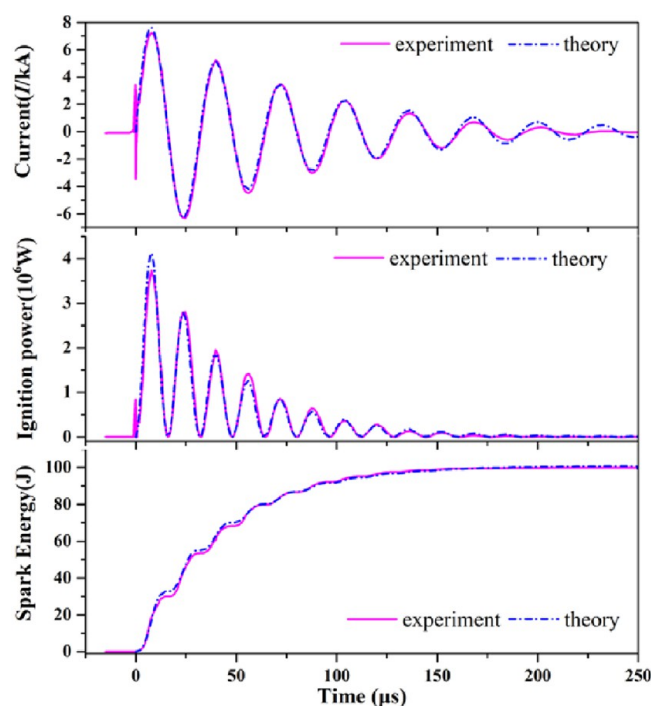


**Figure 2.** Parameter curve of the discharge process with an ignition energy of 100 J.

that the duration time of 100 J spark discharge process is about 250  $\mu$ s. The oscillating discharge power function will be applied in the simulation model.

In order to reflect the ignition process more accurately, an oscillating discharge power function is applied to the ignition area, which was determined as

$$P = 5009760 \times \left[ \exp\left(-\frac{t}{0.00008125}\right) \right]^2 \times \sin^2(196349.54 \times t) \quad (19)$$

It should be noted that the above oscillating discharge power function is the fitting function of experiment results from Figure 2.

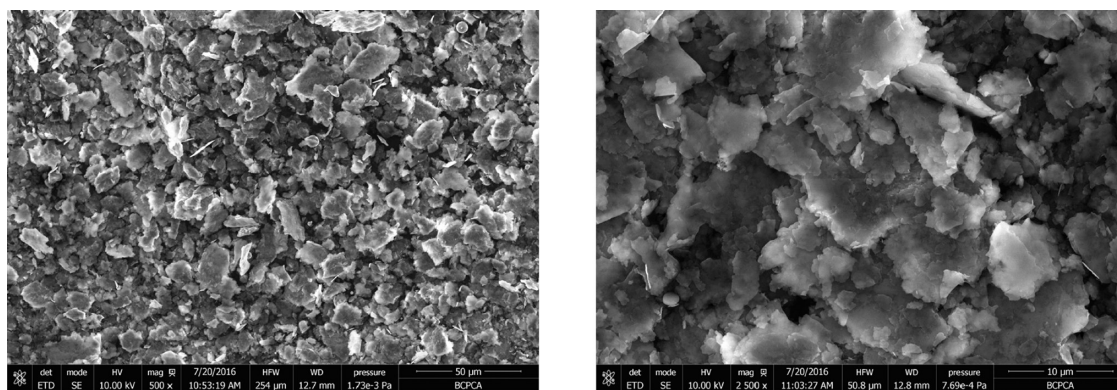


Figure 3. SEM of flake aluminum dust samples.

The container wall and the connecting pipe wall are rigid walls made of stainless steel, and the thermal conductivity is 16.3 W/(m·K). The explosive dust in the container is flake aluminum particles with  $d_{50} = 14.21 \mu\text{m}$ , and its morphology is shown in Figure 3. The detailed physical parameters have been described in previous work.<sup>19,33</sup> According to the equivalent concentration of aluminum dust explosion ( $341 \text{ g/m}^3$  under normal temperature and pressure), the designed simulation scheme is summarized in Table 2.

In order to minimize the interference of mesh generation on simulation results, the verification of mesh independence is a necessary work for numerical simulation. The grid parameters of four different scales are shown in Table 3. As shown in Figure 4,

Table 2. Simulation Condition

case no.	ignition mode	initial dust cloud range	initial dust concentration ( $\text{g/m}^3$ )	total weight of the dust layer in the connecting pipe (g)
case 1	I	large container	100	0
case 2	I	large container	300	0
case 3	I	large container	500	0
case 4	I	large container	700	0
case 5	II	small container	100	0
case 6	II	small container	300	0
case 7	II	small container	500	0
case 8	II	small container	700	0
case 9	I	large container	300	100
case 10	I	large container	300	200
case 11	I	large container	300	500
case 12	I	large container	300	800
case 13	II	small container	300	100
case 14	II	small container	300	200
case 15	II	small container	300	500
case 16	II	small container	300	800

Table 3. Different Meshing Methods

model no.	grid size (mm)	grid number
model 1	25	448245
model 2	20	1020557
model 3	15	2159299
model 4	10	6596256

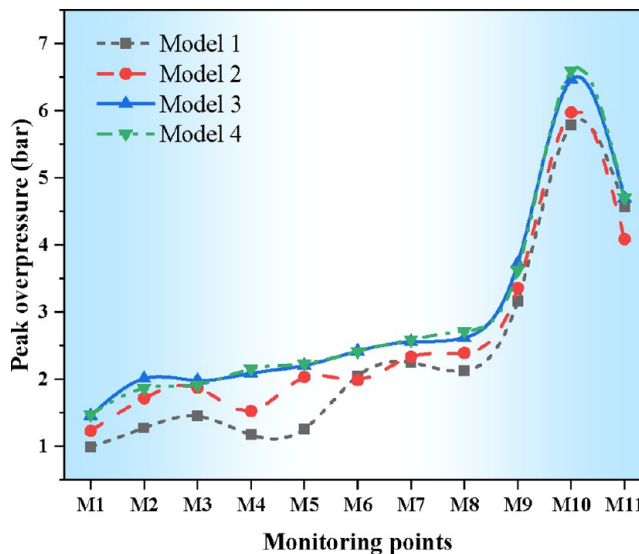


Figure 4. Evolution of peak overpressure for different meshing methods (Case 5 in Table 2).

the peak overpressure of each monitoring point obtained by the four meshing methods is investigated. It can be found that after the mesh size is reduced to 15 mm, the calculation accuracy is not significantly improved by continuing to reduce the mesh size. Therefore, the following work uses the meshing method of Model 3, and the calculation time of each case is about 85 h (CPU: AMD Ryzen 9 5950X 16-Core Processor, 3.40 GHz).

**2.3. Verification of the Numerical Method.** The experimental setup of a 20 L near-spherical explosion system is schematically shown in Figure 5a. It mainly consists of a 20 L explosion container, an electric ignition system, a dust dispersion system, a control unit, and a data acquisition system. The details of the experimental system have been described in a previous study.<sup>33</sup> The data acquisition system is used to record the overpressure histories. As shown in Figure 5b, a simplified 2D axisymmetric model and mesh of the 20 L near-spherical explosion container is built, and the overpressure histories of

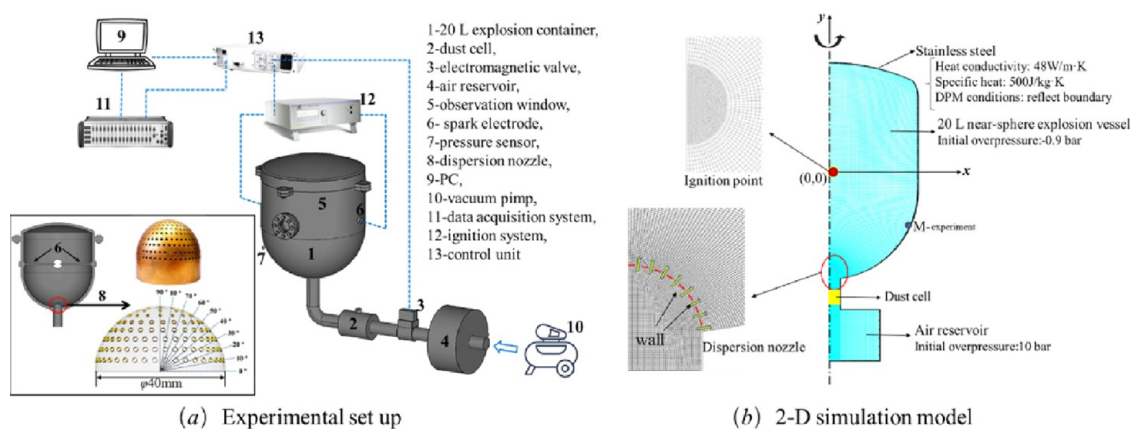
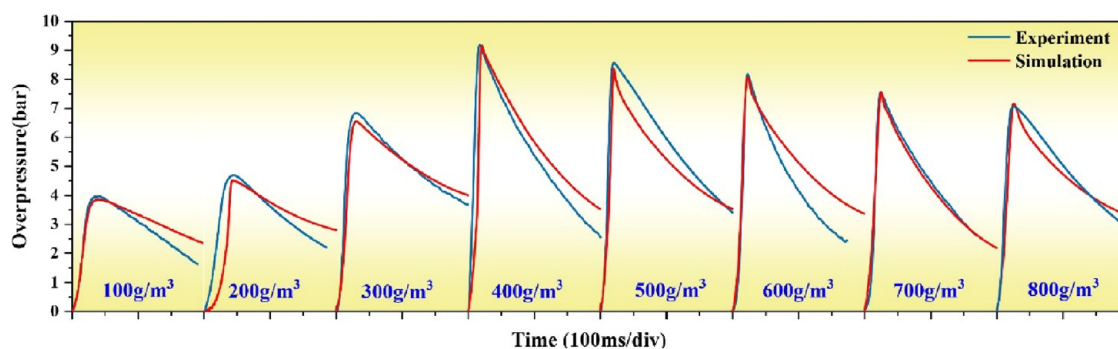
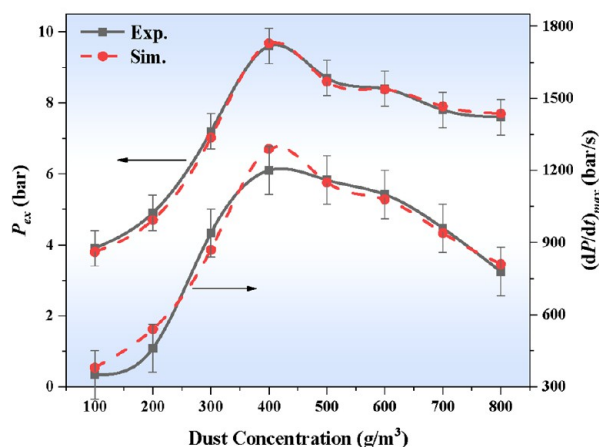


Figure 5. Experimental system and simplified 2D model for the verification of the numerical method.



(a) Explosion overpressure histories of flake aluminum dust.



(b) Comparison of characteristic parameters between experiments and simulation in 20 L near-spherical explosion system.

Figure 6. Verification of the numerical method.

monitoring point M in different concentrations are used to compare with the experimental results.

Figure 6 shows the explosion overpressure histories of flake aluminum dust with different concentrations obtained in the experiment and simulation. It can be found that the simulation results are in good agreement with the experimental results, and the confidence level of relative error in the interval of 1.58~5.64% is 99%. Therefore, the present simulation method and parameters are suitable to study the explosion characteristics of flake aluminum dust. In addition, some information has been added in the revised manuscript, as shown in Figure 6b. The

peak overpressure and the maximum rise rate of overpressure obtained by experiments and simulation are in good agreement.

Proust et al.,<sup>33</sup> Ren et al.,<sup>34</sup> and Janovsky et al.<sup>35</sup> have found that the peak overpressure and maximum pressure rise rate of dust explosion in explosion containers with different volumes are different. Moreover, the dust explosion overpressure in 1 m<sup>3</sup> explosion container is significantly higher than that in the 20 L explosion container. However, they all meet the “cubic law”, and their explosion indexes  $K_{st}$  have good consistency. Therefore, we compared the  $K_{st}$  of 1 and 5 m<sup>3</sup> cylindrical containers in the present work and a 20 L explosive ball in the verification test, as

shown in Figure 7; they have good consistency and reliability. Therefore, the current explosion model and parameters of flake

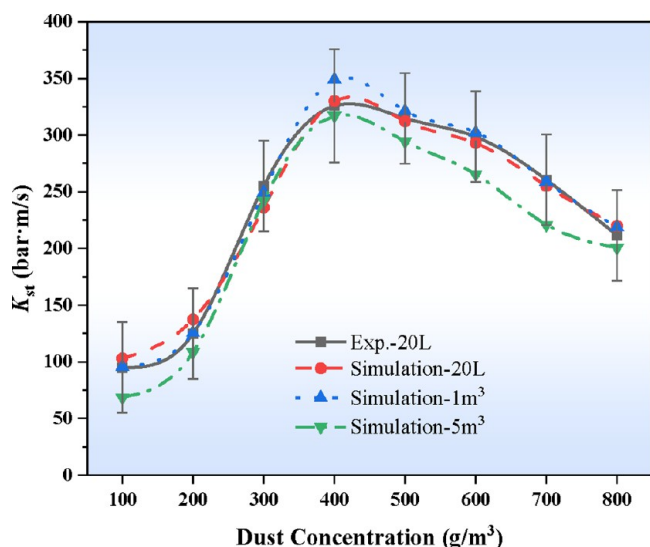


Figure 7. Comparison of the explosion index ( $K_{st}$ ) between 1 m<sup>3</sup>/5 m<sup>3</sup> cylindrical container and 20 L explosion system.

aluminum powder can be used for explosion simulation in 1 m<sup>3</sup>/5 m<sup>3</sup> explosion container.

$$K_{st} = \left( \frac{dP}{dt} \right)_{\frac{1}{3}} \frac{1}{3_{\max}} \quad (20)$$

### 3. RESULTS AND DISCUSSION

**3.1. Influence of Ignition Mode on Explosion Overpressure.** In order to study the influence of ignition mode on explosion propagation process, the cloud diagram of dust explosion overpressure under the two ignition modes (Case 3 and Case 7) is shown in Figure 8. It can be seen that the weak pressure wave (peak overpressure of about 1.5 bar) caused by ignition first propagates outward and then converges to the center of the container after being reflected by the wall. The pressure wave collides with the flame surface, and the exothermic drive of the high-temperature flame generates a stronger pressure wave to propagate outward again. The pressure wave is repeatedly reflected and continuously obtains driving energy from the flame, which leads to the enhancement of pressure wave oscillation in the initiation container. At the same time, the pressure wave propagates to the adjacent container through the connecting pipes and is reflected many times in the adjacent container. The resulting backflow pressure wave causes the turbulence intensity in the detonation container to increase.

As for the ignition mode I (Case 3), the volume of the ignition container is large, and the pressure wave reaches the extreme value in a short time and realizes reverse propagation, so as to enhance the explosion intensity of the detonation container through the jet effect. Therefore, ignition mode I eventually reaches a larger overpressure value in the entire system (about 7 bar).

As for the ignition mode II (Case 7), the pressure wave generated by the small container propagates to the container, which results in the pressure wave propagating in the larger container as pressure relief. The generated reverse pressure wave

is weak and does not significantly enhance the explosion intensity of the detonation container. Finally, the overpressure of the whole system is maintained at a low level, about 3 bar.

Figure 9 shows the pressure wave curves at three representative locations (point 1, point 6, and point 11) for different initial dust concentrations (100, 300, 500, and 700 g/m<sup>3</sup>). It can be found that with the increase of the initial dust concentration, the peak overpressure at each monitoring point increases first and then almost remains stable. The peak overpressure in the detonation container is significantly higher than that of the adjacent container. The detonation container reaches the peak overpressure earlier than the adjacent container, which indicates that the pressure increase of the detonation container is mainly caused by its own explosion heat release and wall constraints. However, the pressure increase of the adjacent container is mainly caused by the increase of the pressure wave oscillation between the two containers, which has a hysteresis. In addition, after crossing the peak point of explosion overpressure, as a whole, because the pressure wave and gas flow oscillate back and forth between the two containers, the pressure in the container rises and falls alternately. Due to the energy loss and wall heat dissipation, the pressure oscillation of the two containers gradually weakens and tends to be consistent. The pressure build-up in the secondary container is mainly due to the oscillating pressure wave going back and forth between the two containers, which has hysteresis.

Figure 10 shows the peak overpressure evolution for different initial concentrations under two ignition modes. The maximum overpressure occurs at the center of the detonation container, which is mainly due to the convergence of the reflected pressure wave from the boundary to the center, resulting in a steep rise of overpressure at the central monitoring point, and the maximum overpressure is higher than 30 bar. In the case of ignition mode I, when the pressure wave propagates into the connecting pipe, the peak overpressure shows a continuous increase trend. This is because the explosion process of large containers lasts for a long time and continuously drives the pressure wave in the pipeline. However, in the case of ignition mode II, the propagation of the pressure wave in the connecting pipe shows a trend of first strengthening and then weakening, which is mainly due to the lower explosion intensity and shorter duration. Therefore, the pressure wave cannot be driven continuously, causing the decrease of peak overpressure when it approaches the explosion relief container. In addition, in ignition mode I, the peak overpressure of the explosion increases when the initial aluminum dust concentration increased from 100 to 500 g/m<sup>3</sup>, and oxygen depletion effect limits the increase in explosion intensity when the initial aluminum dust concentration increased from 500 to 700 g/m<sup>3</sup>. By contrast, when the initial aluminum dust concentration increases to 700 g/m<sup>3</sup>, the explosion peak overpressure still increases under ignition mode II. This is because the back and forth oscillation of pressure wave during the explosion circulates the air to the small container and connecting pipe, which promotes the further reaction of aluminum dust.

**3.2. Influence of Ignition Mode on Flame Propagation Characteristics.** Figure 11 shows the flame propagation process and the distribution of the aluminum dust concentration under the two ignition modes. It can be found that the flame surface appears as a regular fireball in the initial stage, and the aluminum dust particles and products have a clear boundary. Then, due to the convergence and impact of the pressure waves reflected by the wall of the ignition container, and the self-

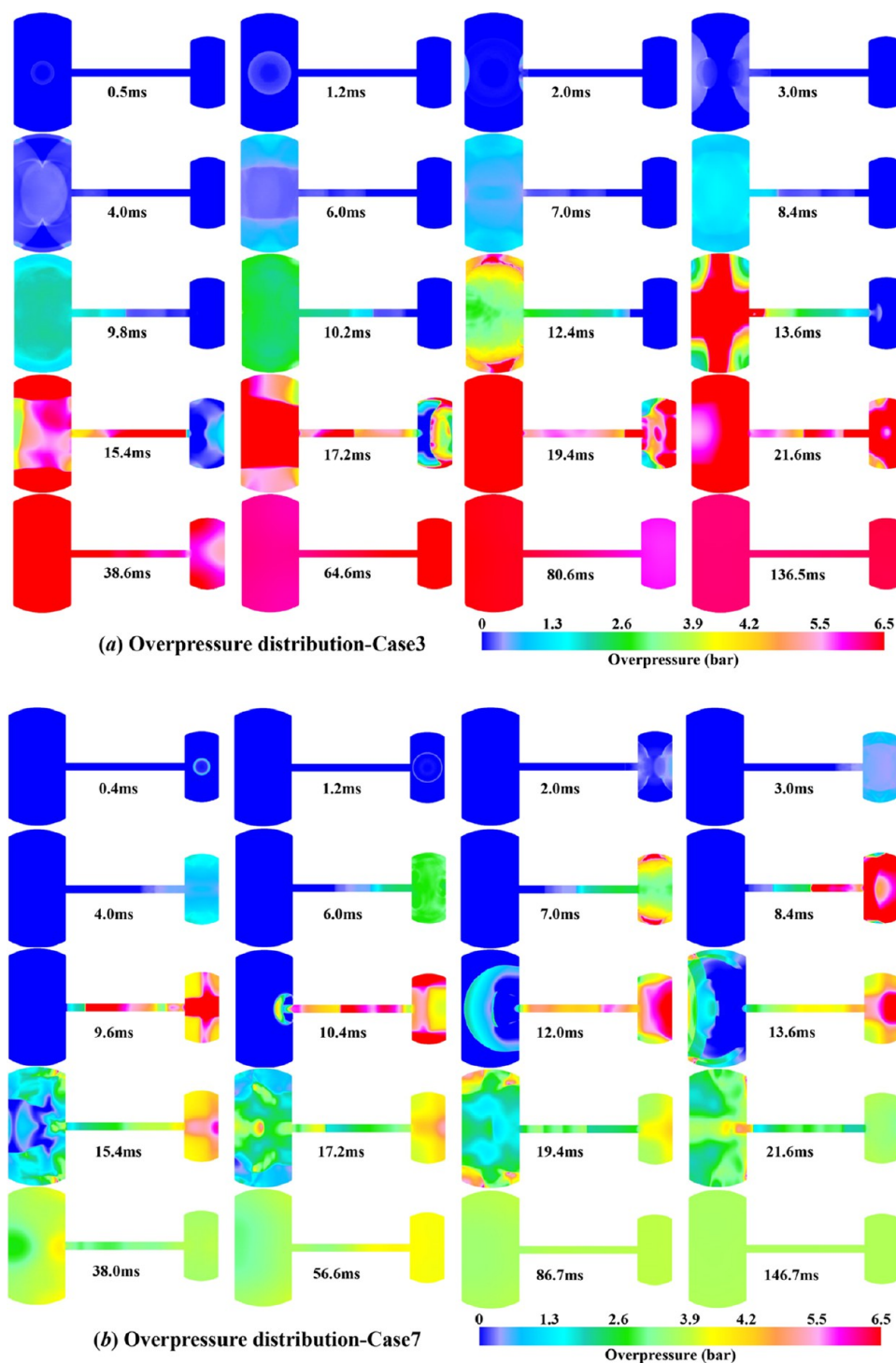
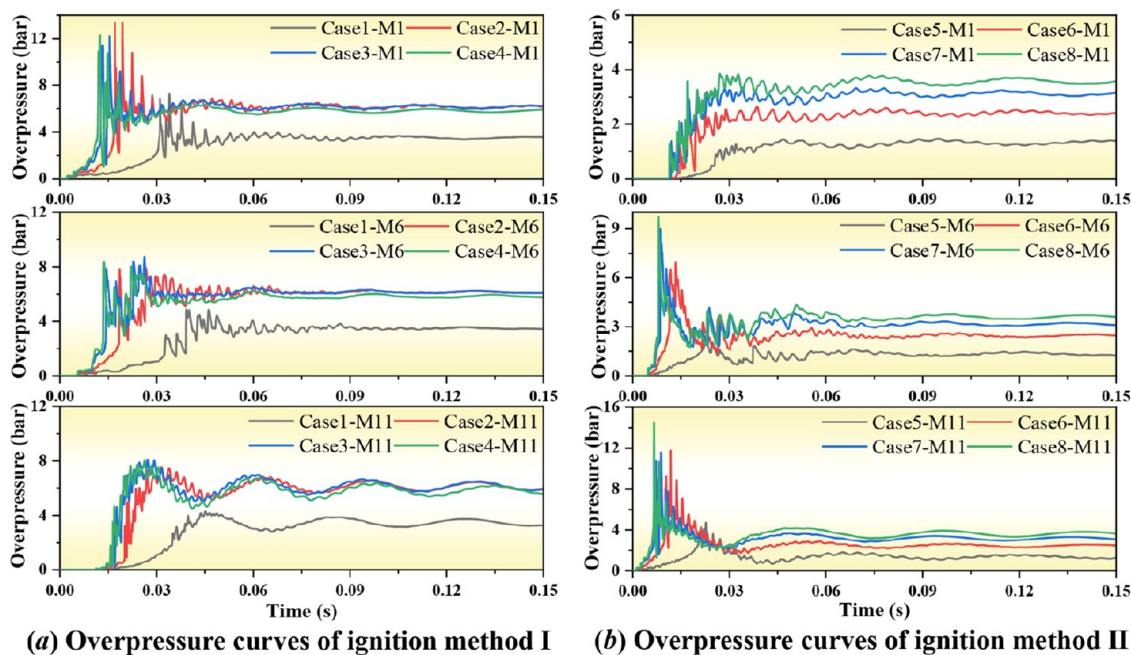


**Figure 8.** Pressure wave propagation process (initial dust concentration is  $500 \text{ g/m}^3$ ).

acceleration mechanism of combustion, the spherical flame gradually transforms into a turbulent flame with a wrinkled surface. The aluminum dust is dragged by the pressure wave and distributed discretely throughout the container. The aluminum dust dragged to the high temperature area causes secondary deflagration and further increases the temperature. Since the propagation speed of the pressure wave is faster than that of the flame front, the aluminum dust is also dragged into the connecting pipe, and the flame surface reaches the connecting pipe to form a jet flame. The aluminum dust in the pipe

continues to participate in the explosion reaction, and the flame is further accelerated.

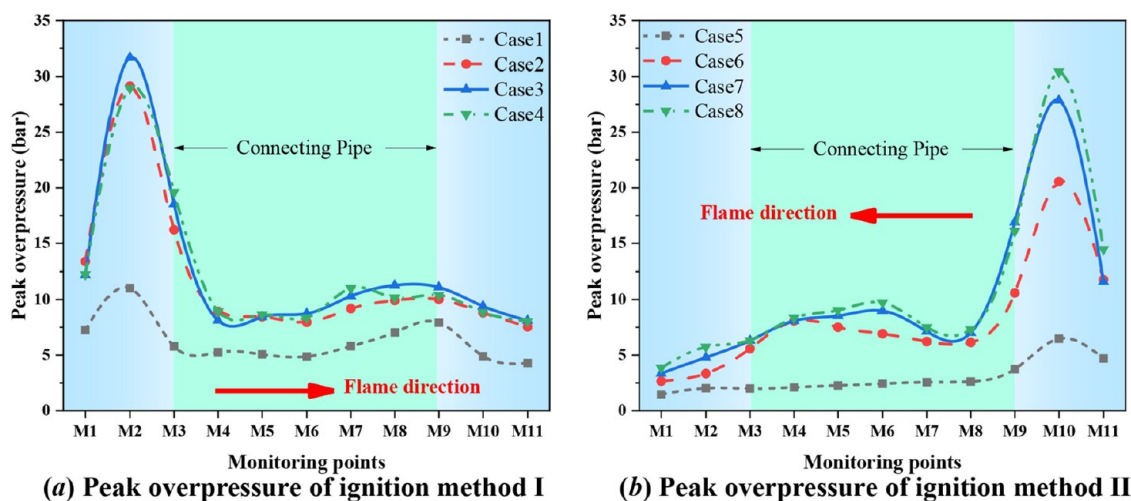
In the case of ignition mode I, when the flame reaches the secondary container, there is still aluminum dust in front of flame surface, so the explosion further develops in the secondary container. However, in the case of ignition mode II, the arrival of the flame surface has completely reacted the aluminum powder in the connecting pipe, and the propagation container is close to an explosion relief container, and the flame intensity gradually weakens.



(a) Overpressure curves of ignition method I

(b) Overpressure curves of ignition method II

Figure 9. Overpressure curves of characteristic monitoring points at different initial concentrations.



(a) Peak overpressure of ignition method I

(b) Peak overpressure of ignition method II

Figure 10. Evolution of peak overpressure at different initial dust concentrations.

Figure 12 shows the temperature curves of each monitoring point during the explosion process with different initial dust concentrations under the two ignition modes. Figure 13 extracts the maximum temperature during flame propagation and the propagation velocity of the flame front. The explosion reaction in the ignition container is relatively sufficient, and the highest temperature appears in the center of the ignition container. Due to the oscillation of the pressure wave, the flame front in the connecting pipeline is alternately stretched and compressed, and the temperature value of the monitoring point in the pipeline has a wide range of steep rise and fall. In the case of ignition mode I, the temperature of the jet flame remains stable in the connecting pipe, and the flame velocity increases slowly. When the flame entered the secondary container, the peak temperature increased significantly. This is because part of the aluminum dust enters the secondary container under the action of the precursor pressure wave, and the flame enters the secondary container and continues to strengthen. Due to the oscillating

propagation of the precursor pressure wave, the flow field in the secondary container is in a high turbulent state, and the explosion reaction is more severe. It should be pointed out that when the initial dust concentration is higher than  $500 \text{ g/m}^3$ , the flame velocity at the end of the connecting pipe exceeds  $900 \text{ m/s}$ , which is a very violent deflagration phenomenon.

In the case of ignition mode II, a large amount of aluminum dust is not dragged into the secondary container. Therefore, the jet flame does not develop further after entering the secondary container, and its temperature remained stable. However, when the flame enters a large-scale container from a narrow pipe, the pressure relief effect causes the flame velocity to increase sharply, exceeding  $800 \text{ m/s}$ . This does not mean that the explosion is further enhanced, but only the hydrodynamic phenomenon of the jet flame in the expanding flow field. As for the peak temperature, the aluminum dust with slightly lower equivalent concentration has the highest peak temperature and the most sufficient combustion. When the initial aluminum dust

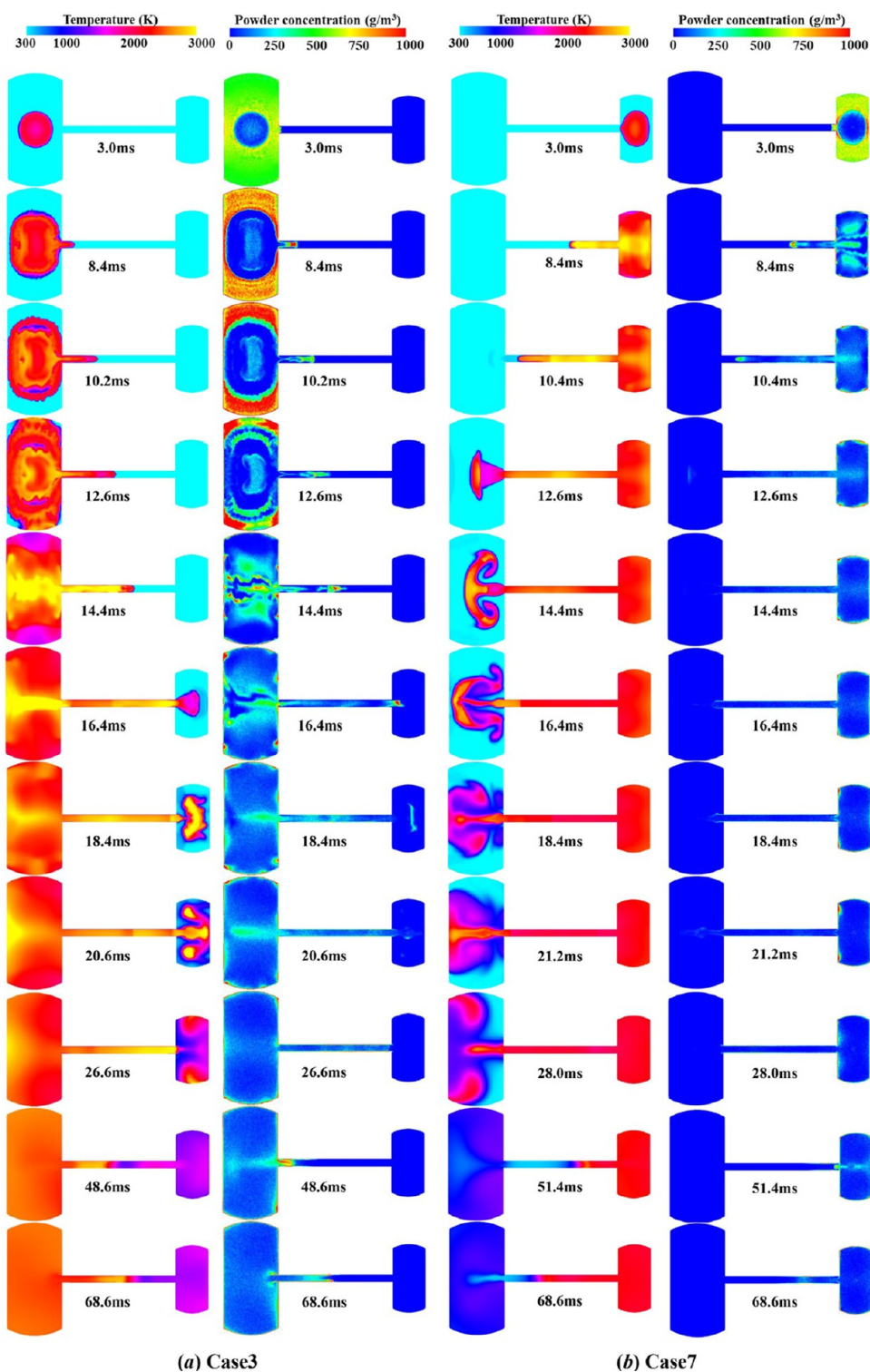


Figure 11. Flame propagation process and dust concentration distribution (initial dust concentration is  $500 \text{ g/m}^3$ ).

concentration is higher than  $300 \text{ g/m}^3$ , the aluminum dust that does not participate in the reaction absorbs part of energy, and the temperature of flow field decreases. In addition, the remaining aluminum dust hinders the diffusion rate of oxygen to the surface of aluminum particles and reduces the reaction rate.

**3.3. Influence of the Dust Layer of the Connecting Pipe on Explosion Overpressure.** Figure 14 shows the pressure wave curves of three characteristic monitoring points

when the aluminum dust layer is laid at the bottom of the connecting pipe, and Figure 15 extracts the peak overpressure of each monitoring point. It can be found that with the increase of the total mass of the accumulated dust layer, the peak overpressure in the detonation container and the secondary container increases. Moreover, the dust layer has little effect on the peak overpressure of the detonation container but has a significant enhancement effect on the peak overpressure of the secondary container. This is mainly due to the fact that the

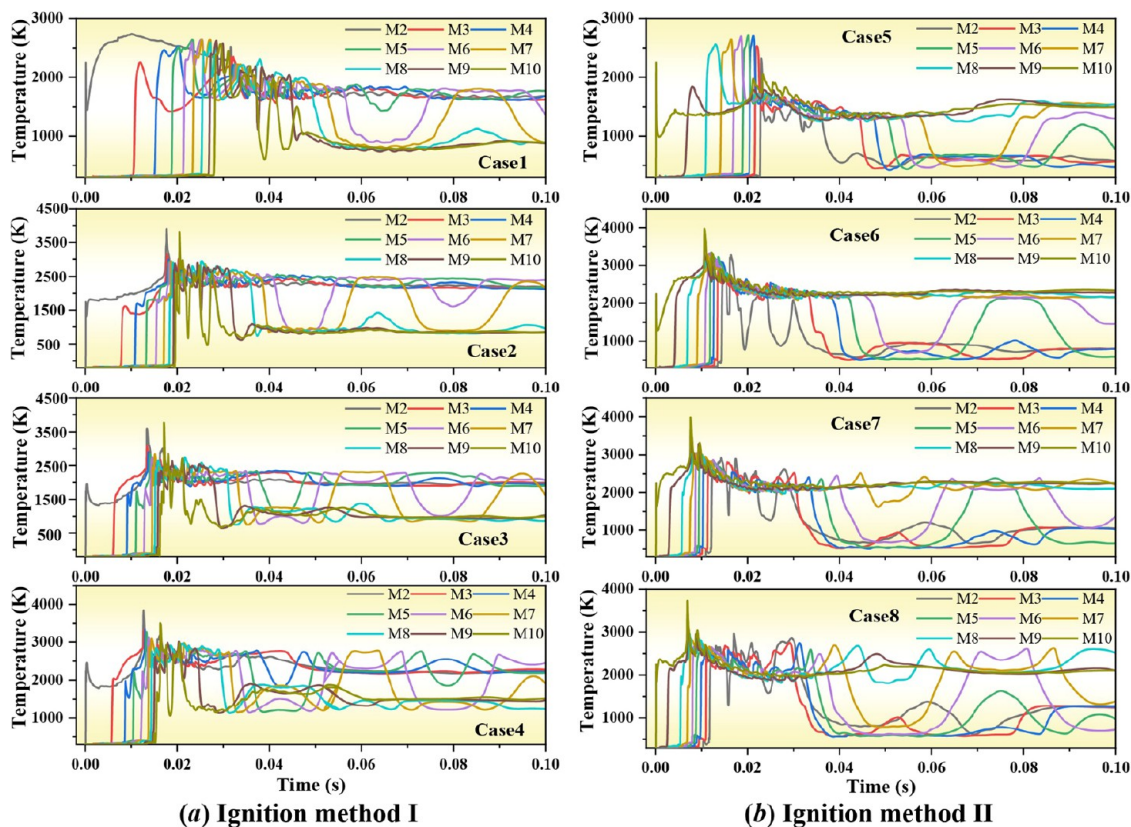


Figure 12. Temperature curves of characteristic monitoring points at different initial concentrations.

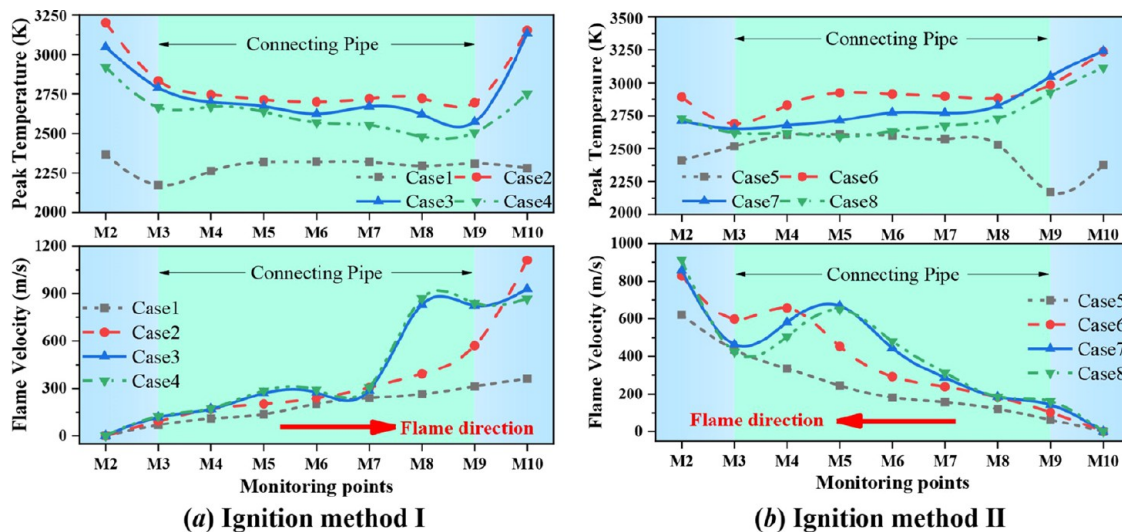


Figure 13. Flame temperature and propagation speed at different initial dust concentrations.

particles of the dust layer are lifted up in the pipe and flow into the secondary container driven by the pressure wave, which makes the explosion develop further in the secondary container. In the case of ignition mode I, the explosion reaches a very violent deflagration state when the explosion propagates to the end of the connecting pipe, and the peak overpressure increases sharply to 30 bar. In addition, in the case of ignition mode II, a similar phenomenon occurs, but the maximum overpressure is only about 20 bar.

### 3.4. Influence of the Dust Layer of the Connecting Pipe on Flame Propagation Characteristics. Figure 16a,b

shows the flame propagation process and the dynamic distribution of 100 and 500 g accumulated dust in the mode I, respectively. Similarly, Figure 16c,d shows the flame propagation process of the 100 and the 500 g dust layer and the dynamic distribution of aluminum dust in the case of ignition mode II, respectively. The dust layer is raised in the connecting pipe under the lifting effect of the precursor pressure wave. After the jet flame enters the connecting pipe, the dust participates in the explosion reaction, which significantly increases the explosion intensity. Due to the action of gravity, the dust concentration in the lower part of the secondary container is

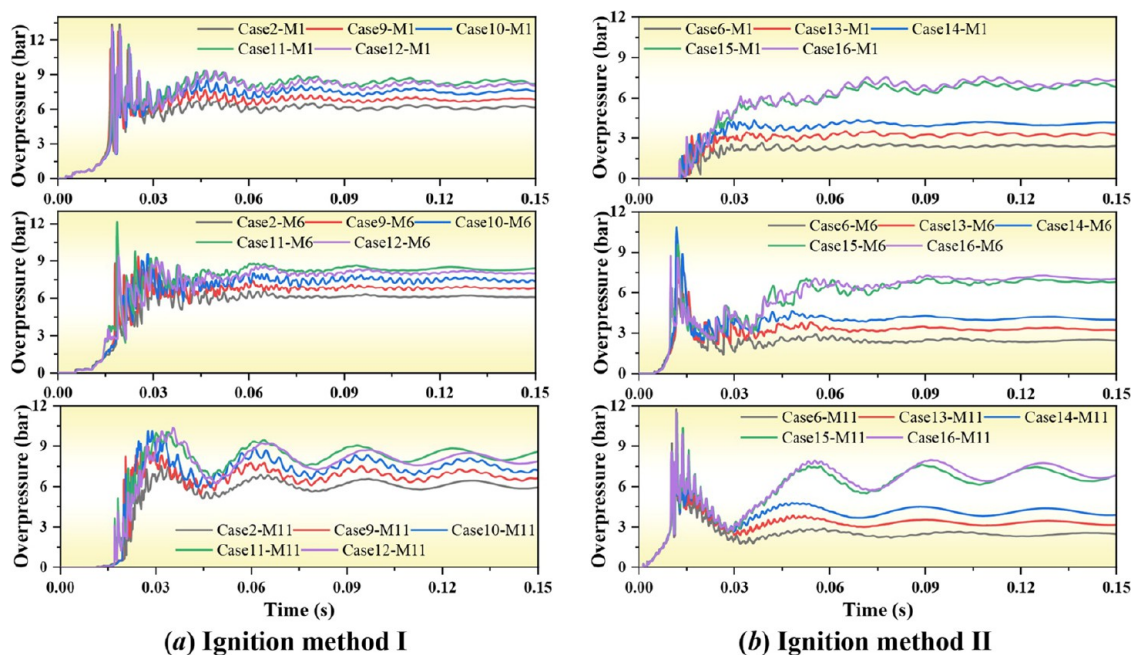


Figure 14. Overpressure curves of characteristic monitoring points in the presence of the dust layer of the connecting pipe.

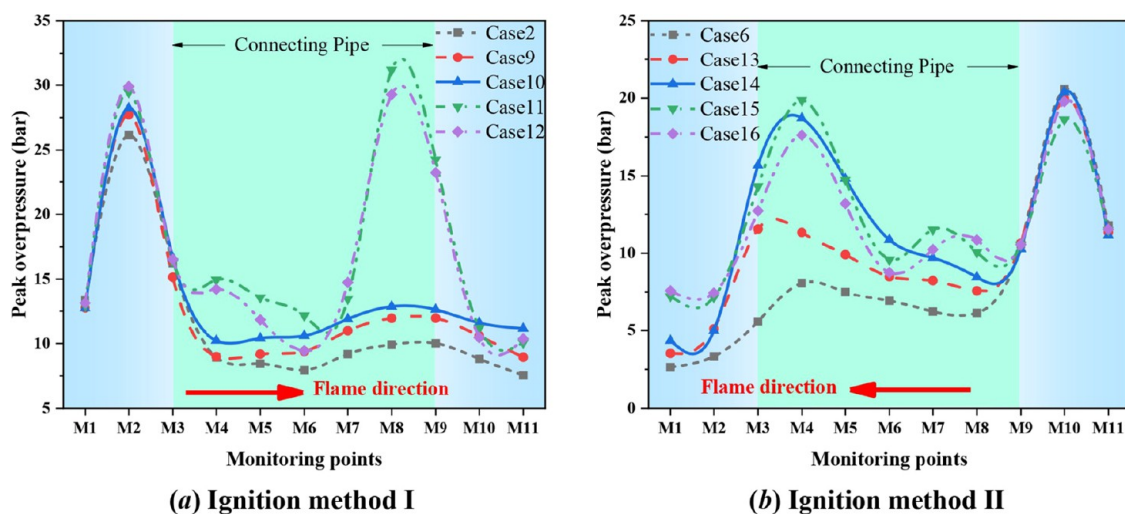


Figure 15. Evolution of peak overpressure in the presence of the dust layer of the connecting pipe.

significantly higher than that in the upper part. After the flame enters the secondary container, the flame gradually fills the entire secondary container. Under the stretching and compression of the oscillating pressure wave, the explosion product is alternately stretched and compressed between the two containers. Finally, the aluminum dust of 100 g dust layer almost completely reacts, while the aluminum dust of 500 g dust layer still has a large amount remaining in the connecting pipe and the secondary container.

Figure 17 shows the comparison of the peak temperature and flame propagation velocity under different mass of the deposited dust layer. It can be found that the mass of the dust layer has no significant effect on the peak temperature and flame propagation velocity in the detonation container. When the deflagration wave propagates in the connecting pipe, the flame temperature drops earlier as the mass of the dust layer increases. This is because a large amount of deposited aluminum dust does not participate in the chemical reaction but absorbs a large amount

of heat through thermal conduction and convection for self-heating. When the jet flame enters the secondary container, with the increase of the dust layer mass, the flame temperature under the two ignition modes shows different trends. When the ignition occurs in the large container, the peak temperature of the secondary container shows a decreasing trend. However, when the ignition occurs in the small container, the peak temperature of the secondary container shows a trend of first decreasing and then increasing. This is because when ignition occurs in a large container, a strong shock wave enters the connecting pipe and raises a lot of deposited dust, and a large amount of dust enters and fills the smaller secondary container. When the amount of deposited dust reaches 500 g, there is aluminum dust left in the secondary container, which does not participate in the explosion reaction but absorbs heat, so the peak temperature of the flow field decreases.

However, when the ignition occurs in a small container, the generated precursor pressure wave is weak and does not have an

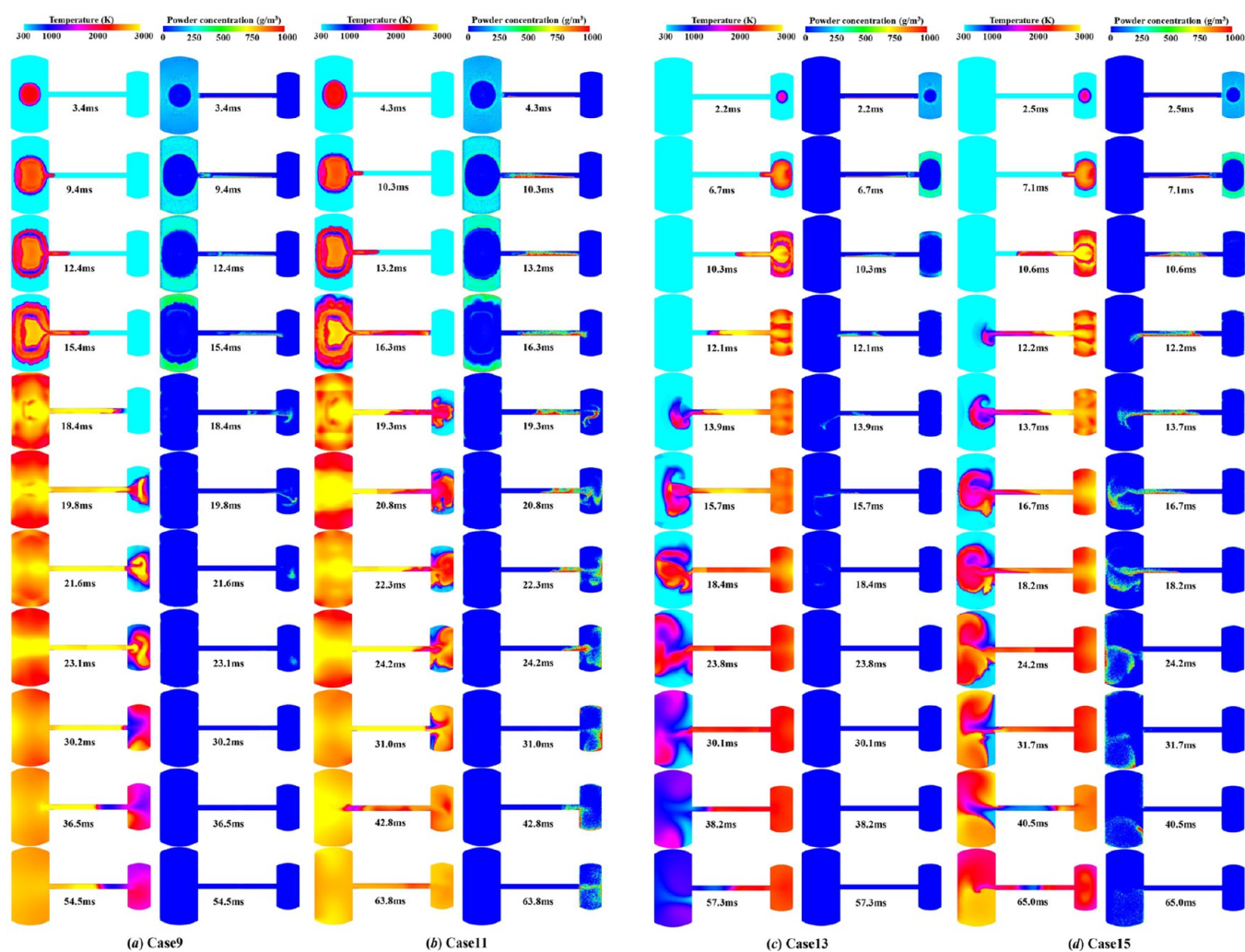


Figure 16. Flame propagation and dust concentration distribution under the influence of the accumulated dust layer.

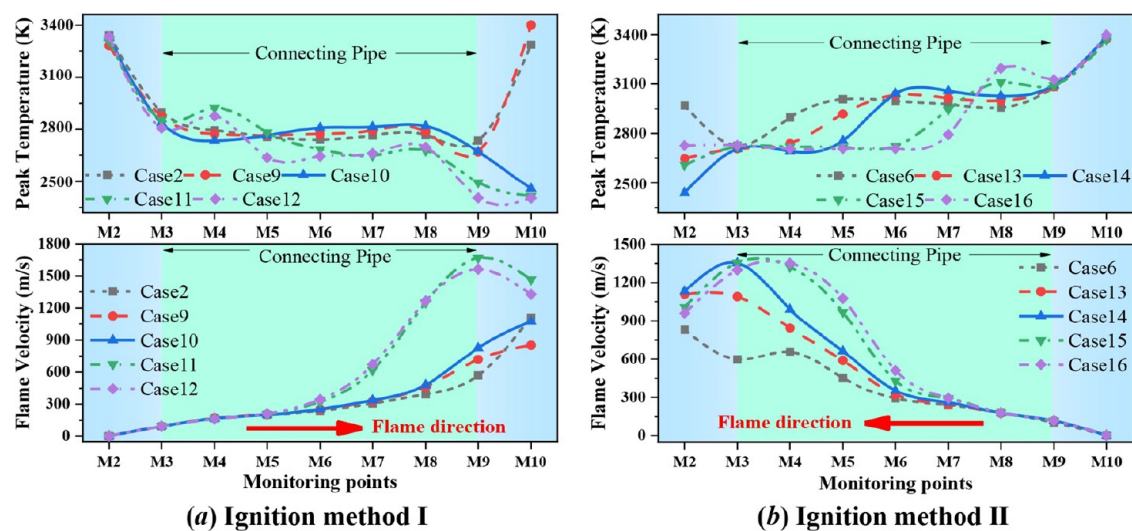
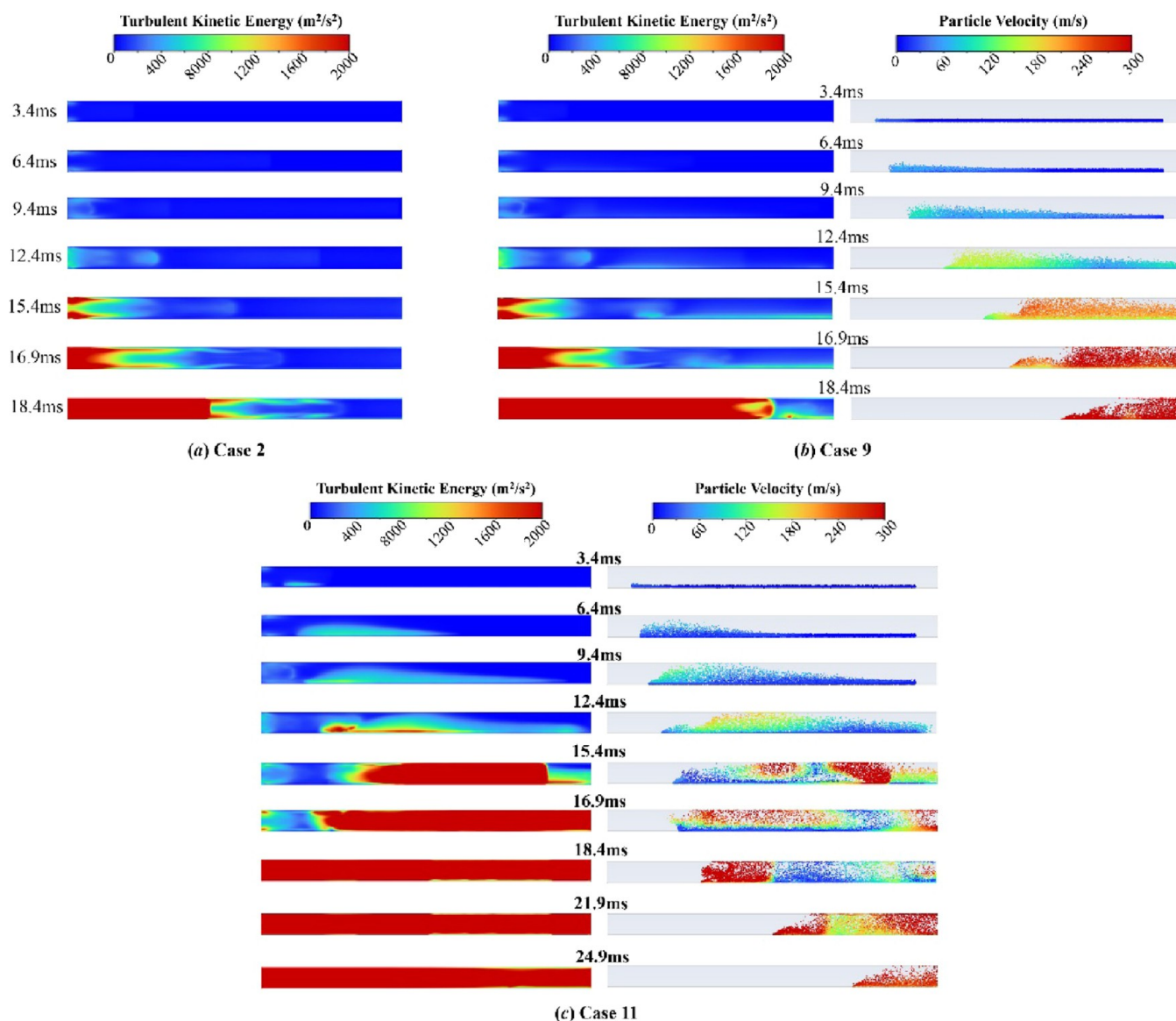


Figure 17. Evolution of flame temperature and flame propagation velocity under the influence of the accumulated dust layer.

effective blowing effect on the dust in the connecting pipe. The dust layer mainly enters the secondary container by horizontal driving force. Therefore, a large amount of aluminum dust is concentrated in the lower part of the larger secondary container. As the amount of deposited dust increases, the amount of

remaining aluminum dust that does not participate in the explosion reaction increases, and the peak temperature at the monitoring point gradually decreases. In addition, the evolution of the flame velocity under the two ignition modes shows a similar law: with the increase of the amount of deposited dust,



**Figure 18.** Particle velocity and turbulent kinetic energy of the flow field in the connecting tube.

the propagation velocity of the flame in the connecting pipe increases gradually. The maximum flame speed can reach 1500 m/s when ignition occurs in a large container, and the maximum flame speed can reach 1350 m/s when ignition occurs in a small container. In other words, the jet flame velocity is increased by 3 times with the participation of the accumulated dust layer. This reveals that as the amount of accumulated dust increases, the propagation speed of the explosion in the connecting pipe is significantly increased, and the danger is greatly enhanced.

Before the flame propagates to the connecting pipe, the dust layer has formed turbulence under the action of pressure wave. In order to further understand the turbulent action mechanism of the deposited dust layer on the explosion overpressure and flame propagation characteristics, the turbulent kinetic energy distribution and particle velocity in the connecting tube are simulated, and the results are shown in Figure 18. It can be found that when there is no dust layer accumulation (Case 2), the turbulent kinetic energy of the flow field only advances synchronously with the propagation of the flame front. When there is a dust layer at the bottom of the connecting pipe, the dust is lifted under the action of the precursor pressure wave, and

the maximum particle velocity is higher than 300 m/s. The longitudinal lifting of particles significantly enhanced the turbulent kinetic energy in the connecting tube, which further enhanced the explosion intensity in the connecting tube and accelerated the flame propagation. When the amount of dust deposited in the connecting pipe increases to 500 g (Case 11), the thickness of the dust layer is large, and the precursor pressure wave is not enough to lift all the dust layers, and the particle velocity being lifted is about 100 m/s. However, the concentration of dust cloud in the deposition tube increases, which makes the turbulent kinetic energy of the flow field increase sharply, thus greatly enhancing the explosion intensity.

#### 4. CONCLUSIONS

In present work, an interconnected system consisting of two cylindrical containers with different volumes and a connecting pipe is established to study the propagation characteristics of aluminum dust explosions. Moreover, the influence of the aluminum dust layer deposited in the connecting pipe on the

explosion propagation is studied. The following conclusions are revealed:

- (1) When ignition occurs in a large container, the pressure wave reflects and oscillates in a short time, which in turn enhances the explosion intensity of the ignition container due to the jet effect. However, when the ignition occurs in a small container, the pressure wave spreads in the larger secondary container, showing a significant pressure relief effect.
- (2) The flame front reaches the connecting pipe to form a jet flame, and the aluminum dust are dragged into the pipe by the precursor pressure wave. Moreover, the flame is further accelerated as the aluminum dust continues to participate in the explosion reaction. The pressure build-up in the secondary container is mainly due to the oscillating pressure wave going back and forth between the two containers, which has hysteresis.
- (3) As the total mass of the aluminum dust layer in the connecting pipe increases, the peak overpressure in both the detonation container and the secondary container increases. Compared with the detonation container, the thickness of the dust layer has a more obvious enhancement effect on the peak overpressure of the secondary container.
- (4) When the ignition occurs in a large container, the dust layer is lifted in the connecting pipe under the action of the precursor pressure wave. After the jet flame enters the connecting pipe, the lifted aluminum dust participates in the explosion reaction, which significantly increases the explosion intensity. However, when the ignition occurs in a small container, the generated precursor pressure wave is weak, and only a small amount of deposited dust enters the secondary container under the action of horizontal thrust.

## AUTHOR INFORMATION

### Corresponding Author

**Yulong Cheng** – Beijing Key Laboratory of Metro Fire and Passenger Transportation Safety, China Academy of Safety Science and Technology, Beijing 100012, China; [orcid.org/0000-0002-5892-2126](https://orcid.org/0000-0002-5892-2126); Email: [akymhz@126.com](mailto:akymhz@126.com)

### Authors

**Dan Wang** – Beijing Key Laboratory of Metro Fire and Passenger Transportation Safety, China Academy of Safety Science and Technology, Beijing 100012, China

**Qi Jing** – State Key Laboratory of Explosion Science and Technology, Beijing Institute of Technology, Beijing 100081, China

Complete contact information is available at:  
<https://pubs.acs.org/10.1021/acsomega.2c06408>

### Author Contributions

<sup>§</sup>D.W. and Q.J. are co-first authors and contributed equally.

### Notes

The authors declare no competing financial interest.

## ACKNOWLEDGMENTS

This work was supported by the National Natural Science Foundation of China (Grant No. 52204244).

## REFERENCES

- (1) Olugbemide, D. I. A CFD study of the effects of pipe bending angle on pressure piling in coal dust explosions in interconnected vessels. *Fire Saf. J.* **2022**, *128*, No. 103540.
- (2) Razus, D.; Oancea, D.; Chirila, F.; Ionescu, N. I. Transmission of an explosion between linked vessels. *Fire Saf. J.* **2003**, *38*, 147–163.
- (3) Kosinski, P.; Hoffmann, A. C. Mathematical modelling of dust explosions in interconnected vessels. *Nonlinear Anal.* **2005**, *63*, No. e1087.
- (4) Wang, Z. R.; Pan, M. Y.; Jiang, J. C. Experimental investigation of gas explosion in single vessel and connected vessels. *J. Loss Prev. Process Ind.* **2013**, *26*, 1094–1099.
- (5) Hashimoto, A.; Matsuo, A. Numerical analysis of gas explosion inside two rooms connected by ducts. *J. Loss Prev. Process Ind.* **2007**, *20*, 455–461.
- (6) Ogungbemide, D.; Clouthier, M. P.; Cloney, C.; Zalosh, R. G.; Ripley, R. C.; Amyotte, P. R. Numerical modelling of the effects of vessel length-to-diameter ratio (L/D) on pressure piling. *J. Loss Prev. Process Ind.* **2021**, *70*, No. 104398.
- (7) Huang, C.; Bloching, M.; Lipatnikov, A. N. A vented corn starch dust explosion in an 11 . 5 m 3 vessel : Experimental and numerical study. *J. Loss Prev. Process Ind.* **2022**, *75*, No. 104707.
- (8) Zhang, Q.; Yu, Y.; Li, Y.; Chen, Z.; Jiang, J. Coupling effects of venting and inerting on explosions in interconnected vessels. *J. Loss Prev. Process Ind.* **2020**, *65*, No. 104132.
- (9) Yin, Z.; Wang, Z.; Zhen, Y.; Cao, X.; Jiang, K.; Ma, S. Propagation Characteristics of Gas Explosion in Linked Vessels Based on DDT Criteria. *J. Loss Prev. Process Ind.* **2021**, *73*, No. 104598.
- (10) Li, H.; Guo, J.; Yang, F.; Wang, C.; Zhang, J.; Lu, S. ScienceDirect Explosion venting of hydrogen-air mixtures from a duct to a vented vessel. *Int. J. Hydrogen Energy* **2018**, *43*, 11307–11313.
- (11) Cui, Y. Y.; Wang, Z. R.; Ma, L. S.; Zhen, Y. Y.; Sun, W. Influential factors of gas explosion venting in linked vessels. *J. Loss Prev. Process Ind.* **2017**, *46*, 108–114.
- (12) Zhang, Q.; Jiang, J.; You, M.; Yu, Y.; Cui, Y. Experimental study on gas explosion and venting process in interconnected vessels. *J. Loss Prev. Process Ind.* **2013**, *26*, 1230–1237.
- (13) Kosinski, P.; Hoffmann, A. C. An investigation of the consequences of primary dust explosions in interconnected vessels. *J. Hazard. Mater.* **2006**, *137*, 752–761.
- (14) Reding, N. S.; Shiflett, M. B. Consequence prediction for dust explosions involving interconnected vessels using computational fluid dynamics modeling D v. *J. Loss Prev. Process Ind.* **2020**, *65*, No. 104149.
- (15) Boeck, L. R.; Bauwens, C. R.; Dorofeev, S. B. Modeling of explosion dynamics in vessel-pipe systems to evaluate the performance of explosion isolation systems. *J. Loss Prev. Process Ind.* **2021**, *71*, No. 104477.
- (16) Sun, W.; Liu, L.; Li, Y.; Huang, C.; Chen, X.; Feng, M. Insight into vented explosion mechanism and premixed flame dynamics in linked vessels : Influence of membrane thickness and blocking rate. *J. Loss Prev. Process Ind.* **2021**, *72*, No. 104581.
- (17) Song, Y.; Zhang, Q. Multiple explosions induced by the deposited dust layer in enclosed pipeline. *J. Hazard. Mater.* **2019**, *371*, 423–432.
- (18) Wang, D.; Ji, T.; Jing, Q.; He, W.; Fan, Z.; Wu, D.; Qian, X. Experimental study and mechanism model on the ignition sensitivity of typical organic dust clouds in O<sub>2</sub>/N<sub>2</sub>, O<sub>2</sub>/Ar and O<sub>2</sub>/CO<sub>2</sub> atmospheres. *J. Hazard. Mater.* **2021**, *412*, No. 125108.
- (19) Jing, Q.; Wang, D.; Liu, Q.; Shi, C.; Liu, J. Ignition sensitivity and explosion behaviors of micron-sized aluminum powder: Comparison between flake aluminum powder and spherical aluminum powder. *Chem. Eng. Sci.* **2022**, *252*, No. 117502.
- (20) Jing, Q.; Wang, D.; Liu, Q.; Ren, L.; Wang, Y.; Liu, C.; Shen, Y.; Wang, Z. Study on transient reaction mechanism and explosion intensity parameters of micron-sized flake aluminum dust in air. *Chem. Eng. Sci.* **2021**, *246*, No. 116884.
- (21) Jing, Q.; Wang, D.; Liu, Q.; Chen, X.; Shen, Y.; Wang, Z.; Zhong, Y. Inhibition effect and mechanism of ultra-fine water mist on CH<sub>4</sub> /

air detonation: Quantitative research based on CFD technology. *Process Saf. Environ. Prot.* **2021**, *148*, 75–92.

(22) Kosinski, P.; Hoffmann, A. C. Dust explosions in connected vessels: Mathematical modelling. *Powder Technol.* **2005**, *155*, 108–116.

(23) Song, Y.; Zhang, Q. Criterion and propagation process of spark-induced dust layer explosion. *Fuel* **2020**, *267*, No. 117205.

(24) Song, Y.; Nassim, B.; Zhang, Q. Explosion energy of methane/deposited coal dust and inert effects of rock dust. *Fuel* **2018**, *228*, 112–122.

(25) Pang, L.; Zhang, Z.; Cui, S.; Sun, S. Experimental study of the venting characteristics of dust explosion through a vent duct. *J. Loss Prev. Process Ind.* **2020**, *65*, No. 104144.

(26) Pang, L.; Cao, J.; Xiao, Q.; Yang, K.; Shi, L. Explosion propagation in a dust removal pipeline under dust collector explosion. *J. Loss Prev. Process Ind.* **2022**, *74*, No. 104662.

(27) Dong, C.; Bi, M.; Zhou, Y. Effects of obstacles and deposited coal dust on characteristics of premixed methane – air explosions in a long closed pipe. *Saf. Sci.* **2012**, *50*, 1786–1791.

(28) Liu, L.; Zhang, Q. Comparison of detonation characteristics for typical binary blended fuel. *Fuel* **2020**, *268*, No. 117351.

(29) Li, J.; Zeng, F.; Chen, S.; Zhang, K.; Yan, C. Acta Astronautica Bayesian model evaluation of three  $k-\omega$  turbulence models for hypersonic shock wave–boundary layer interaction flows. *Acta Astronaut.* **2021**, *189*, 143–157.

(30) Jing, Q.; Wang, D.; Liu, Q.; Shen, Y.; Wang, Z.; Chen, X.; Zhong, Y. Transient reaction process and mechanism of cornstarch/air and  $\text{CH}_4$ /cornstarch/air in a closed container: Quantitative research based on experiments and simulations. *J. Hazard. Mater.* **2021**, *409*, No. 124475.

(31) Jing, Q.; Liu, Q.; Wang, D.; Shen, Y.; Wang, Z. Calculation model for drag coefficient and multi-phase flow characteristics in dust removal process: Comparison between flake aluminum powder and spherical aluminum powder. *Powder Technol.* **2022**, *405*, No. 117550.

(32) Wang, D.; Qian, X.; Wu, D.; Ji, T.; Zhang, Q.; Huang, P. Numerical study on hydrodynamics and explosion hazards of corn starch at high-temperature environments. *Powder Technol.* **2020**, *360*, 1067–1078.

(33) Proust, C.; Accorsi, A.; Dupont, L. Measuring the violence of dust explosions with the “20 l sphere” and with the standard “ISO 1 m<sup>3</sup> vessel”: Systematic comparison and analysis of the discrepancies. *J. Loss Prev. Process Ind.* **2007**, *20*, 599–606.

(34) Ren, J.; Chang, C.; Rao, G.; Bai, C.; Jing, Q.; Peng, X.; Xiao, Q. Experimental and numerical simulation study on the effect of ignition delay time on dust explosion in the 1 m<sup>3</sup> vessel. *J. Loss Prev. Process Ind.* **2022**, *78*, No. 104801.

(35) Janovsky, B.; Skrinsky, J.; Cupak, J.; Veres, J. Coal dust, Lycopodium and niacin used in hybrid mixtures with methane and hydrogen in 1 m<sup>3</sup> and 20 l chambers. *J. Loss Prev. Process Ind.* **2019**, *62*, No. 103945.